**Mantle Phase Changes and Deep-Earthquake Faulting in Subducting Lithosphere**

Stephen H. Kirby; William B. Durham; Laura A. Stern

*Science*, New Series, Vol. 252, No. 5003 (Apr. 12, 1991), 216-225.

Stable URL:
http://links.jstor.org/sici?sici=0036-8075%2819910412%293%3A252%3A5003%3C216%3AMPCADF%3E2.0.CO%3B2-G

*Science* is currently published by American Association for the Advancement of Science.

---

Your use of the JSTOR archive indicates your acceptance of JSTOR's Terms and Conditions of Use, available at http://www.jstor.org/about/terms.html. JSTOR's Terms and Conditions of Use provides, in part, that unless you have obtained prior permission, you may not download an entire issue of a journal or multiple copies of articles, and you may use content in the JSTOR archive only for your personal, non-commercial use.

Please contact the publisher regarding any further use of this work. Publisher contact information may be obtained at http://www.jstor.org/journals/aaas.html.

Each copy of any part of a JSTOR transmission must contain the same copyright notice that appears on the screen or printed page of such transmission.

---

JSTOR is an independent not-for-profit organization dedicated to creating and preserving a digital archive of scholarly journals. For more information regarding JSTOR, please contact jstor-info@umich.edu.

http://www.jstor.org/
Thu Mar 11 19:39:36 2004

# Mantle Phase Changes and Deep-Earthquake Faulting in Subducting Lithosphere

STEPHEN H. KIRBY, WILLIAM B. DURHAM, LAURA A. STERN

**Inclined zones of earthquakes are the primary expression of lithosphere subduction. A distinct deep population of subduction-zone earthquakes occurs at depths of 350 to 690 kilometers. At those depths ordinary brittle fracture and frictional sliding, the faulting processes of shallow earthquakes, are not expected. A fresh understanding of these deep earthquakes comes from developments in several areas of experimental and theoretical geophysics, including the discovery and characterization of transformational faulting, a shear instability connected with localized phase transformations under nonhydrostatic stress. These developments support the hypothesis that deep earthquakes represent transformational faulting in a wedge of olivine-rich peridotite that is likely to persist metastably in coldest plate interiors to depths as great as 690 km. Predictions based on this deep structure of mantle phase changes are consistent with the global depth distribution of deep earthquakes, the maximum depths of earthquakes in individual subductions zones, and key source characteristics of deep events.**

MANY CRYSTALLINE COMPOUNDS, INCLUDING MANY MINerals, transform to denser phases only with increasing pressures (*1*). Subduction zones (SZs) provide a splendid natural laboratory for the study of pressure-induced phase transformations under nonhydrostatic stress. In SZs the lithosphere, Earth's cold boundary layer, is thrust deep into the mantle. Each year, 80 to 120 $km^3$ of lithosphere descend below 350 km while being progressively pressurized and slowly heated. Experimental studies indicate that a sequence of solid-solid phase transformations occur during slab descent (*2, 3*). Discontinuities occur in seismic velocities at depths of about 400, 520, and 670 km (*4, 5*) (Fig. 1). These discontinuities correspond closely to the pressures at which olivine ($\alpha$ phase) (*6*) of approximate composition $(Mg_{0.1}Fe_{0.9})_2SiO_4$ is expected to transform to modified spinel structure ($\beta$ phase), $\beta$ phase transforms to spinel ($\gamma$ phase) and, at greater pressure, spinel ($\gamma$ phase) transforms to magnesiowüstite (Mw) plus $(Mg,Fe)SiO_3$ perovskite (Pv) (*2, 3*), respectively. Because the descending lithosphere is thick and a poor thermal conductor, it can remain anomalously cold for millions of years during active subduction. It may be as much as 1000°C cooler than the surrounding mantle (*7, 8*). This thermal structure, confirmed by seismic measurements to >350 km depth (*9*), is expected to alter the depths at which transformations occur in subducted lithosphere compared to normal mantle and to reduce the rates of thermally activated processes, such as phase transformations and plastic deformation.

The primary geophysical expression of colder temperatures in SZs are anomalously deep earthquakes. A cold descending slab can evidently support sufficient nonhydrostatic stress to permit faulting within the slab, whereas normal mantle with higher ambient temperatures cannot. The earthquakes are distributed in inclined, sheetlike forms that extend to depths as great as 690 km (*10, 11*). These SZ earthquakes decrease in numbers with depth (Fig. 1) from a maximum near the surface to a relative minimum at a depth of about 300 km and then increase from 300 to 400 km to a peak at about 600 km before abruptly decreasing to zero at depths greater than about 684 to 691 km (*12–16*).

An enigma accompanies the occurrence of sudden faulting at pressures of 10 to 24 GPa at those depths (*17–20*). Most shallow earthquakes occur by ordinary fracture and frictional sliding on existing fractures, consistent with direct observations of earthquake ruptures and laboratory data at low to moderate temperatures and low pressures (*20*). However, both fracture strength and resistance to frictional sliding increase steeply with normal stress and depth and exceed the deviatoric stresses required for ductile flow of most rocks at pressures generally less than 1 GPa and temperatures of 400 to 700°C. Ductile behavior is thus expected at pressures of 10 to 24 GPa. Fluid pressure can extend the depth range of brittle fracture by reducing effective normal stresses and may account for seismic activity at depths to 300 km (*19, 21*). The presence of free fluids in interconnected porosity is unlikely, however, below 350 km. A host of alternative physical mechanisms for deep unstable faulting have been proposed (*17, 20, 22, 23*), including shear melting and plastic creep instabilities, but none satisfy both the seismic observations and the requirement that the faulting instability occur under pressure-temperature conditions found deep in SZs.

Most deep seismic activity occurs between the depths of the major seismic discontinuities at 400 and 670 km (Fig. 1). This observation has fueled speculation that phase changes are somehow responsible for the occurrence of deep events (*8, 24–30*). The early hypothesis that rapidly running implosive phase changes in metastable minerals occurred consequent to pressurization at low temperature (*25*) was rejected because the expected dilatational first motions are inconsistent with the radiation patterns of earthquakes (*17, 31*), as described below. The possibility of low-pressure upper-mantle minerals existing metastably at very high pressures in the cold descending lithosphere has recently been revived (*30, 32, 33*). Metastable phases might transform fast enough to radiate elastic wave energy if

S. H. Kirby and L. A. Stern are in the Branch of Tectonophysics, U.S. Geological Survey, Mail Stop 977, 345 Middlefield Road, Menlo Park, CA 94025. W. B. Durham is in the Experimental Geophysics Group of the Earth Sciences Department, Lawrence Livermore National Laboratory, University of California, Box 808, Livermore, CA 94550.

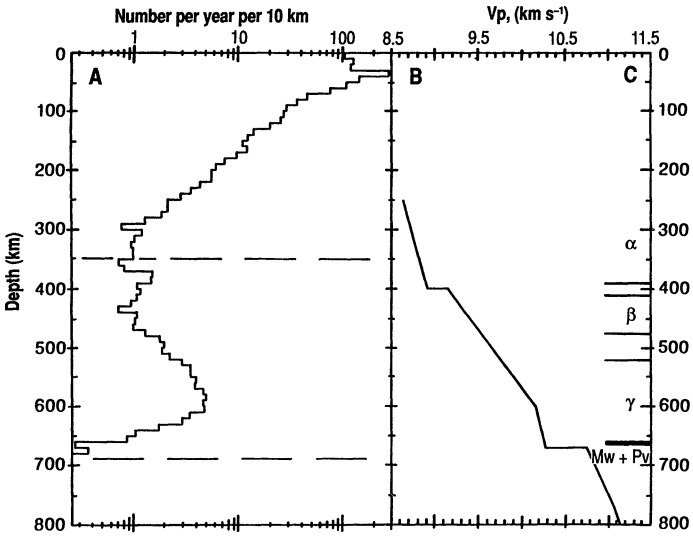


**Fig. 1.** (**A**) Histogram of the worldwide depth distribution of earthquakes (magnitude >5) (*12*). (**B**) Variation of compressional wave velocity with depth in the mantle. From the PREM model of Dziewonski and Anderson (*4*). (**C**) Expected equilibrium depths of mantle phase transformations for olivine bulk composition $(Mg_{0.89},Fe_{0.11})_2SiO_4$ based on the phase diagram and geotherm of Akaogi *et al.* (*3*). The velocity increase for the $\beta \rightarrow \gamma$ transition is too small and broad to be detectable in the PREM model.

sufficiently overdriven in pressure. This hypothesis has not provided an explanation of why the seismic radiation patterns are dominated by shear. Moreover, there was no experimental evidence for shear instabilities caused by solid-solid phase changes under stress.

A clearer understanding of a possible connection between phase transformations and deep earthquakes has recently emerged from work in experimental rock mechanics, petrology, seismology, and modeling of SZs. These developments include the discovery and characterization of a new type of shear instability connected with localized phase transformations under nonhydrostatic stress (*18, 19*). This faulting process, termed transformational faulting (*18*), is facilitated by high pressure, unlike brittle fracture and frictional sliding. A unified and self-consistent hypothesis of deep earthquakes has emerged from these developments. According to this model, phase changes are inhibited in the coldest interiors of slabs, and thus olivine can persist metastably in a wedge-shaped structure that is sandwiched by warmer lithosphere that has already transformed to denser phases during descent. This wedge is subject to wedge-parallel compressive stresses because of the volume compression taking place around it. It can then fail by transformational faulting involving the olivine-spinel transformation localized in the fault zones. We describe the work that leads to this hypothesis and explore its implications for deep earthquakes and the mechanics of deep subduction.

## Characteristics of Deep Earthquakes

Any viable hypothesis of the genesis of deep earthquakes must be compatible with their general characteristics. Most deep earthquakes occur in lithosphere that is either subducting at high rates or is old (*7, 27, 29, 34, 35*). A number of deep rogue events also occur that are located hundreds of kilometers from active SZs (*12*). Deep seismicity in individual SZs generally starts at depths greater than 300 to 350 km (*36*). At least six SZs have earthquakes deeper than 650 km, but no earthquake has been located with confidence at depths greater than 691 ± 10 km (*12, 13*) (Fig. 1). Radiation patterns of deep earthquakes involve movements indicative of shear displacements on faults (*37–39*) (the so-called "double-couple" mechanism, referring to a system of forces involving two mutually perpendicular force couples). The stress state of the lithosphere inferred from these radiation patterns is predominantly down-dip compression (*12, 38, 40, 41*). Faulting as a source process is also consistent with planar zones of deep seismicity cutting across a given slab (*11, 38, 42*), and source directivity along such zones suggest that faults grow progressively (*43*). Isotropic (volume change) components of the wave fields of deep events are too small to detect with the use of current methods (*12, 44*). Deep earthquake sources are not very different from shallow events except that they propagate at less than the shear-wave velocity (*12*). Deep earthquake waveforms suggest that the rise times for these events are shorter than for shallow and intermediate-depth earthquakes (*45*). Unlike most shallow earthquakes, deep events do not have numerous smaller aftershocks that decay in number with time and are located on the main shock rupture surface (*37, 46*).

## Transformational Faulting in Ice

Phase transformations in $H_2O$ ice provide an attractive nonmetallic model system for the investigation of the effects of nonhydrostatic stresses on reconstructive polymorphic transformations and for understanding how phase changes relate to inelastic processes such as faulting. Reconstructive transformations (*47*) predominate in the mantle (*2*). The ice I→II transformation [Fig. 2A; (*48*)] is an archetypical example of a reconstructive polymorphic phase transition with large volume change (−20.2% at 195 K and 173 MPa). Ice I displays many, if not all, of the inelastic properties and processes of single-phase silicates and other rock-forming minerals (*49–51*). As in our earlier work (*49–51*), we shortened cylindrical polycrystalline ice samples at approximately fixed rates while they were simultaneously under a constant confining pressure $P_c$ and temperature $T$. The differential stress supported by the sample is $\sigma = \sigma_1 - P_c$, where $\sigma_1$ is the maximum principal compressive stress directed along the cylinder axis. Ice II was retained in a metastable state by cooling under pressure (*52*). The soft indium jackets that seal the samples were peeled from most samples, and used as replicas of the cylindrical sample surfaces. These replicas reveal the distribution of ice II because the ice I→II volume change creates surface relief.

The I→II transformation becomes increasingly sluggish at temperatures below about 215 K, and hydrostatic pressures exceeding the equilibrium pressures are required for the transformation to run to completion during the time under pressure (50 to 300 s) (*50*). This kinetic limit of ice I metastability increases more or less exponentially with decreasing temperature (Fig. 2A). We observed two types of macroscopic phenomena (*49*) under nonhydrostatic conditions at confining pressures below the kinetic limit (Fig. 2): (i) bulk homogeneous transformation to ice II at high temperatures and (ii) heterogeneous transformation expressed as transformational faulting (*18*). The bulk transformation process determines the upper temperature and normal stress limits for transformational faulting.

*Bulk transformation under nonhydrostatic stress.* Samples shortened 9 to 10% at conditions near the hydrostatic-kinetic limit partially transformed to ice II. Transformation was homogeneous on the whole-specimen scale, and most of the permanent strain was caused by the I→II volume change. Practically all the volumetric change occurred by axial shortening with nearly zero radial strain. Samples deformed in this high-temperature regime had low yield strengths and transiently low strengths beyond yield compared to samples deformed at lower pressures in the ice I stability field, a phenome-

non we attribute mostly to the time-dependent I→II volume change (*49*).

Lens-shaped ice II inclusions oriented preferentially normal to the maximum compressive stress $\sigma_1$ (Fig. 3A) nucleated and grew during deformation and were responsible for most of the inelastic strain sustained by the samples. Displacement and stress fields develop around these flaws because of misfit associated with the reduced volume of the new phase. Similar features have been seen in the $\alpha \rightarrow \gamma$ transformation in deformed $Mg_2GeO_4$ (*19, 53*). Many small microinclusions were located on original ice I grain boundaries; this relation suggests that the flaws nucleate at grain boundaries and grow anisotropically in response to continuous variation in chemical-potential difference around the inclusion under nonhydrostatic stress (*54*). The anisotropy in inclusion growth and in macroscopic transformation strain indicate that the thermodynamic driving potential for the ice I→II transformation $\Delta G$ (the difference in Gibbs free energy between ice I and II at constant temperature) includes the work term $\sigma_1 \Delta V$ instead of $P\Delta V$ (*55*) in the hydrostatic case. Thus the appropriate intensive thermodynamic variable is $\sigma_1$ instead of $P$ (Fig. 2B). Samples that transformed in bulk did so at essentially the same $\sigma_1$ values as the pressures at which undeformed ice I transformed under hydrostatic conditions (Fig. 2B). The kinetic criterion for bulk transformation at a given $T$ therefore depends on the maximum normal stress, $\sigma_1$, and the time under normal stress, for both hydrostatic and nonhydrostatic conditions.

*Transformational faulting.* Transformational faulting only occurred when ice I was carried metastably into the ice II stability field at a low enough temperature and normal stress so that the transformation rate was not fast enough to keep pace with the rate of shortening (Fig. 2B). Differential stresses then rose and failure occurred by faulting. We did not observe any increase in differential stress at failure, $\sigma_f$, with increasing pressure (*56*). Increased pressure did not induce a transition to ductile behavior (Fig. 4A). In the equilibrium stability field of ice II for pressures up to 300 MPa, faulting occurred at a critical shear stress and did not depend on normal stress (Fig. 4B). This critical shear stress varied from ~85 MPa at 77 K to ~53 MPa at 172 K and decreased weakly with deformation rate. No macroscopic fracture surfaces developed in these faulted samples; shear zones were generally cohesive and composed of fine-grained crystalline material that contained ice II (Fig. 5). Faults were typically oriented at about 45° to $\sigma_1$. Faulting produced loud acoustic reports and large drops in differential stress.

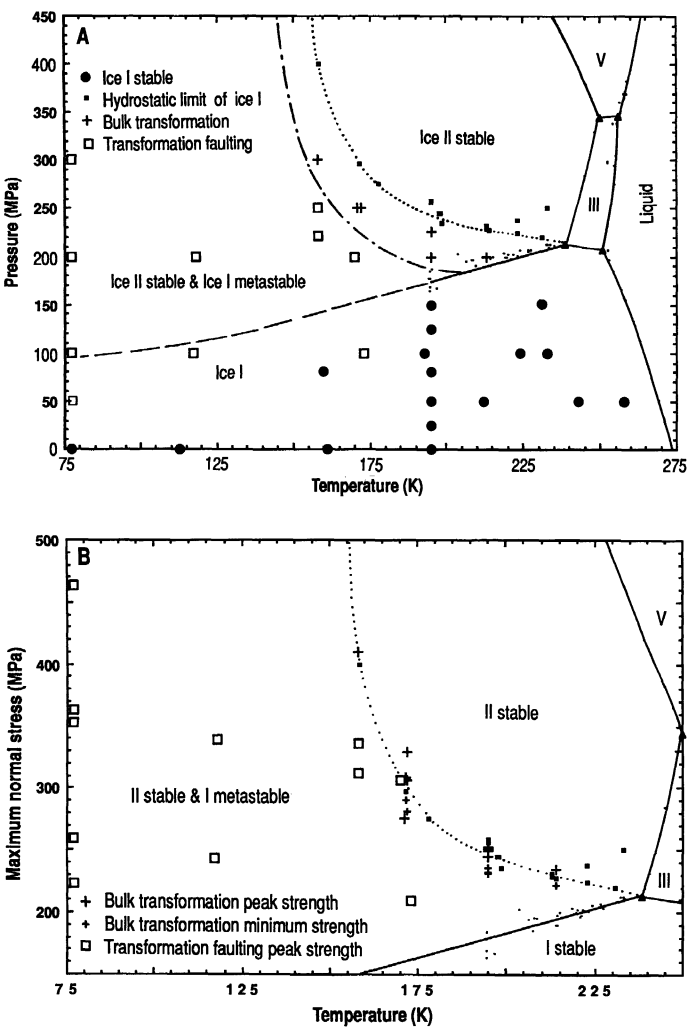


**Fig. 2.** Phase diagrams for water and the physical conditions of the ice experiments. The equilibrium lines (solid) are from Bridgman (*48*) and the kinetic limit that ice I may be carried metastably into the field of ice II (dotted line) is from Durham *et al.* (*50*) and the present work. (**A**) Temperature versus pressure. Points represent the confining pressures and temperatures of the deformation experiments. Strain rate was $3.5 \times 10^{-4}\ s^{-1}$. (**B**) Temperature versus maximum normal stress $\sigma_1$. Note that the $\sigma_1$ values at yield and at 5% strain bracket the metastable kinetic limit of ice I under hydrostatic stress.

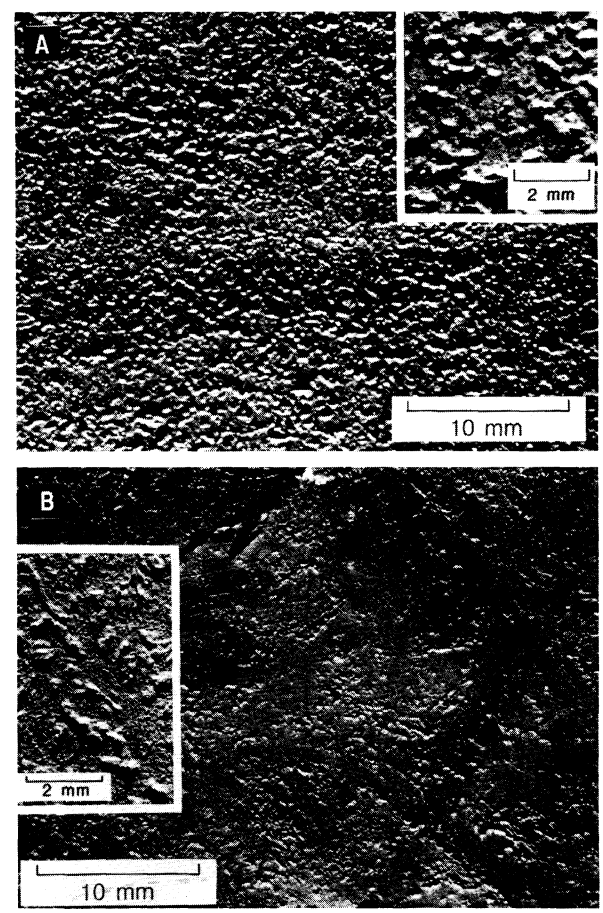


**Fig. 3.** Reflected light micrographs of indium jacket replicas peeled from the external cylindrical surfaces of samples partially transformed to ice II under nonhydrostatic stress. Compression direction and direction of grazing illumination are vertical. Microinclusions of ice II are indicated by raised regions above the background indium. (**A**) Sample transformed in bulk at $T$ = 172 K, $P_c$ = 250 MPa (run 275). Note elongation of the approximately elliptical inclusions in the direction normal to $\sigma_1$. Inset shows magnified view. (**B**) Sample that faulted at $T$ = 119 K and $P_c$ = 200 MPa (run 270). Note the greater complexity in the distribution, shapes and apparent interactions of the ice II inclusions than in (A). Several protofaults inclined to the compression direction are evident. Inset shows magnified view of a protofault composed of an en echelon array of ice II microinclusions. The macroscopic fault cuts the upper left corner of the micrograph.

The samples that faulted showed small departures from elastic behavior just before rapid faulting (Fig. 4A). Microinclusions of ice II nucleated and grew during this inelastic stage before failure (Fig. 3B). The transformation strain calculated from the small volume fraction of ice II microinclusions (<3%) approximately matched the prefault inelastic strain.

Green and Burnley (*19*) proposed that the growth and interactions of compressional microinclusions of spinel in the olivine-structure host under nonhydrostatic stress are responsible for nucleation of transformational faults in $Mg_2GeO_4$, a process that evidently applies to ice as well. Our evidence (Fig. 3B) is essentially the same as theirs: small, inelastic deformation preceded faulting, ice II microinclusions occurred in every faulted sample, microinclusions show evidence of stress interaction, and protofaults composed of arrays of inclusions were seen in many samples. Also, transformational faults commonly cut microinclusions; this relation indicates that the inclusions predate fault nucleation and growth. The microinclusions were much more complex in orientation and shape than those produced during bulk transformation at higher temperatures (Fig. 3B). Many microinclusions in the faulted samples were nonplanar, and some were extended in directions that correspond to planes that were subjected to high shear stress (Fig. 3B). Our observations lead us to the conclusion that under the larger deviatoric stresses in the transformational faulting regime, ice II microinclusions grow in response to the maximum normal stress and the local shear stress, and that these inclusions interact to nucleate transformational faults.

Localization of transformation and shear strain that develops rapidly after fault nucleation can promote fault growth. Some of the likely softening processes that enhance reaction kinetics at the tips of growing faults are (*18*): (i) The new phase can be weaker than the host phase. We rule out this explanation because ice II of the same grain size as ice I is slightly stronger. In faulting observed at higher pressures (*56*) transformation to a potentially soft amorphous phase may have occurred. (ii) Ice II in the fault zone is very fine grained. A number of creep processes are favored by fine grain size, including superplastic behavior associated with grain boundary sliding (*18, 19, 35, 57*). (iii) During fast growth of transformational faults, the release of latent heat can be a destabilizing factor in the feedback between viscous heating and temperature-dependent deformation and reaction rates. The direct effect on the driving potential $\Delta G$ is a reduction through the entropy term. Temperature effects on reaction kinetics can, however, overwhelm the effect on $\Delta G$ (*58*) and produce a net increase in reaction rates. (iv) Volume changes associated with phase transitions also effect rheology and plasticity (*59*).

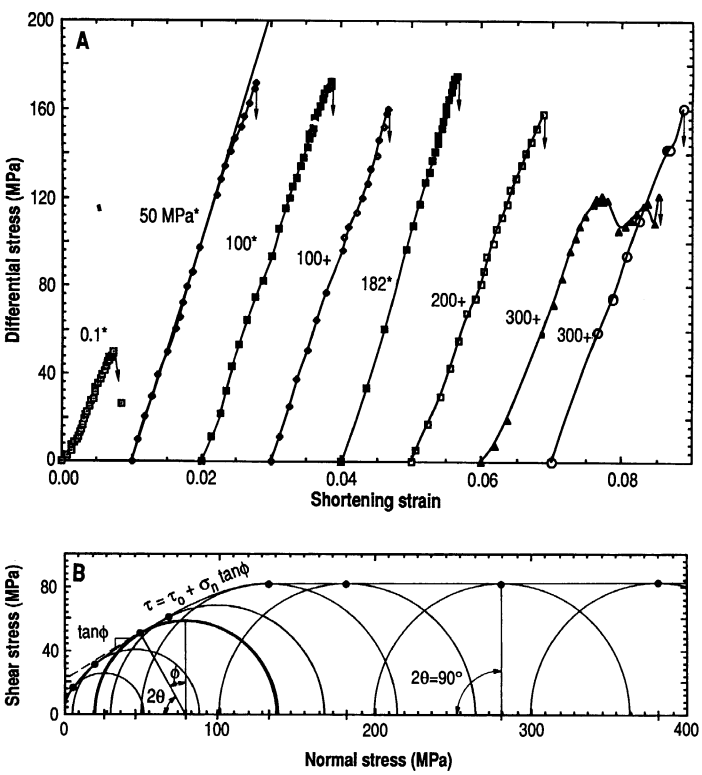


**Fig. 4.** Effects of pressure on the faulting strengths of ice at 77 K. (**A**) Stress-strain curves of samples deformed at various confining pressures; *, strain rate of $3.5 \times 10^{-4}\ s^{-1}$; +, strain rate of $3.5 \times 10^{-6}\ s^{-1}$. Experiments all terminated by faulting. Note lack of increase in failure strength with increasing confining pressure. (**B**) Mohr diagram showing the stress state at failure for experiments at 77 K, including those in (A). The locus of shear stresses and normal stresses on planes inclined by angle θ to the compression direction is a circle. The limiting values of shear and normal stresses at failure, the Mohr envelope (curved line tangent to the Mohr circles), is independent of normal stress above about 100 MPa, indicating that the faulting process is strictly a shear instability. $\phi'$ is the angle of internal friction.

## Reconstructive Phase Transformations in Other Materials

Transformation faulting has been found in two other non-metallic compounds: tremolite (*18, 60*), which transforms to diopside plus talc at high pressures (*61*), and, as noted above, $Mg_2GeO_4$ in the olivine structure (*19*). Faulting in tremolite at high pressure has many properties in common with transformation faulting in ice. One difference, however, is that exploratory electron diffraction data suggest that in the experiments, tremolite transformed to an amorphous phase in the fault zone (*62*). We therefore do not include tremolite in the thermodynamic analysis that follows because we are not confident of the properties of the transformation. Meade and Jeanloz (*63*) reported acoustic emissions from serpentine samples compressed and heated in a diamond-anvil apparatus. They proposed that these emissions are connected to the rapid formation of an amorphous phase and that this is the physical mechanism of deep earthquakes. They have not demonstrated that these acoustic events are connected with faulting. The data for tremolite and the evidence that transformational faulting in ice in experiments above 300 MPa

**Fig. 5.** Sample that faulted at high pressure (run 263, $T$ = 77 K and $P_c$ = 100 MPa) cut perpendicular to the fault plane. Fault is inclined at about 45° to $\sigma_1$. Cohesion is maintained and the shear zone contains fine-grain ice II, which scatters light more than the host ice I, and therefore appears bright. Fractures radiating from the fault probably occurred when the jacket ruptured and the inert fluid confining medium entered the sample under load.

may be associated with production of an amorphous phase (*56*) does suggest that transformational faulting may be responsible for the acoustic emissions that they observe. Deep events occur as much as 50 km into the interiors of subducting plates (*11, 42*), not just near the top of the slab where hydrous minerals should be most abundant. This observation makes it doubtful that transformation to an amorphous phase is involved in most deep earthquakes.

Recent studies (*19*) on $Mg_2GeO_4$ olivine germanate demonstrate that transformational faulting occurs in a system closer in structure to mantle phases. Faulting behavior in germanate has many striking similarities to that in ice. Faulting in the germanate occurred at stresses of 50 to 1200 MPa compared to 106 to 170 MPa in ice, depending on temperature and strain rate. Fine-grained spinel was observed in the fault zones. A transition to bulk transformation occurred at high temperature. Below about 1100 K, ductile deformation occurred without a change of state. We have not observed this lower temperature limit in ice, but we have not done experiments at temperatures below 77 K.

The faults in the germanate were inclined at about 30° to the compression direction in contrast to 45° in ice. This difference may stem from differences in the mechanism by which transformational faults grow. Green and co-workers (*19*) emphasized that microinclusions must nucleate and grow in a region in order for a fault to propagate by inclusion-inclusion stress interactions and coalescence [see also Geller (*64*)]. In contrast, Kirby (*18*) suggested that the faults grow, once nucleated, by a process of stress-assisted transformation kinetics. Brittle faults have been shown to grow by intense microfracturing at the edge of the fault (*65*). Reches and Lockner (*66*) pointed out that the stress field of a pair of closely spaced en echelon tensile cracks can lead to new tensile cracks at locations that extend the inclined array and ultimately can localize shear displacement within the array. We observed en echelon arrays of ice II inclusions in which each inclusion was inclined to $\sigma_1$ (inset, Fig. 3B). Some arrays traversed otherwise inclusion-free ice and some crosscut earlier inclusions. In that the stress fields of tensile cracks and microinclusions are similar (*19*), growth of the transformational faults may occur by a process like that envisioned by Reches and Lockner but with the lens-shaped flaws oriented more nearly perpendicular to $\sigma_1$, as observed in ice (Fig. 3A). The stress effects on inclusion growth kinetics may be different in the ice I→II and the $Mg_2GeO_4$ $\alpha\rightarrow\gamma$ phase changes and hence influence faulting angle. Such a self organization of transformation flaws at the tip of a growing fault is a more credible model of fault growth than one that requires a distribution of microinclusions in a region before faulting can propagate through it, particularly at larger scales in SZs.

Transformational faulting does not occur in all materials that transform reconstructively under stress. As discussed above, latent heat and volumetric changes are important factors in the growth of ice II microinclusions and in the localization of strain in transformational faults. These factors vary considerably among phase transformations (*67*) (Fig. 6). Seven nonmetallic compounds that transform reconstructively to denser phases have been studied under nonhydrostatic stresses: Ice I, tremolite, $Mg_2GeO_4$ olivine, calcite (*68*), α-quartz (*69*), albite (*70*), and rubidium iodide (*71*). The transformations associated with faulting in the laboratory, the $\alpha\rightarrow\gamma$ $Mg_2GeO_4$ olivine and ice I→II transformations, have markedly higher latent heat effects than those that do not fault, such as the calcite→aragonite and α-quartz→coesite transformations (Fig. 6). An exception is the reaction of albite to jadeite plus quartz (*72*). Transformations like the one in albite require diffusive separation of components, and are likely to be sluggish relative to those that do not involve diffusion (*73*). This relation between mechanical behavior and the energetics of phase changes points to latent heat as a possible factor in determining whether unstable faulting occurs in a particular transformation.

## Mantle Phase Changes and Stresses in the Descending Lithosphere

In cool subducting lithosphere, the first high-pressure phase expected in the olivine fraction of the mantle during subduction is spinel (γ phase), and the pressure and depth range over which β is stable is narrower in cool subducted lithosphere than at higher temperatures (Fig. 7). All the equilibrium boundaries between α, β, and γ phases have positive Clapeyron slopes. At equilibrium, the denser phases should therefore be stable at shallower depths in the subducting lithosphere than in the surrounding mantle (Fig. 8) (*7, 8*).

Sung and Burns (*32*) pointed out that such a distribution is unlikely in the cold core of subducting lithosphere because reaction rates are likely to be so slow that olivine can persist metastably to depths far below the equilibrium boundaries. They suggested that below ~700°C, olivine may survive to depths greater than 600 km (Figs. 7 and 8). Recent studies have confirmed that reaction rates of the $\alpha\rightarrow\gamma$ transformation are strongly temperature dependent (*19, 74–79*). Rubie *et al.* (*76*) showed that cool temperatures not only greatly reduce the mobilities of interphase boundaries but also can markedly reduce nucleation rates of spinel at host-phase grain boundaries (*76, 80*). They concluded that the pressures required to transform olivine to its denser spinel polymorphs at low temperatures should greatly exceed the equilibrium pressures (*76*), in support of the hypothesis of Sung and Burns. Further support comes from recent seismic observations from earthquakes as deep as 500 km in the Pacific plate subducting beneath Japan (*64, 81*). These observations involve rays traveling up the dip of the slab, increasing the sensitivity to slab-parallel velocity anomalies. The kinetic wedge model of Sung and Burns provides a far better fit to the observed travel time anomalies than a model with an equilibrium distribution of spinel.

Just how far the $\alpha\rightarrow\beta$ and $\alpha\rightarrow\gamma$ transformations may be overdriven below 500 km is not certain. The kinetic line of Sung and Burns (Fig. 7) is approximately consistent with kinetic data on silicate olivine (*74*), and rate data on the $\alpha\rightarrow\gamma$ $Ni_2SiO_4$ transforma-

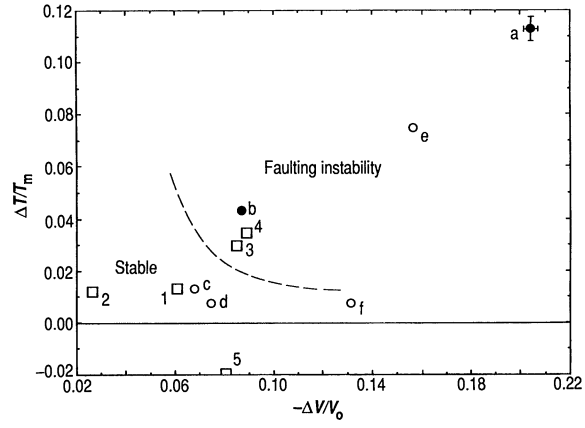


**Fig. 6.** Volumetric strains versus relative temperature changes attributed to latent heat effects for reconstructive phase transformations in nonmetallic compounds. Circles indicate systems that have been studied under nonhydrostatic stress and the filled circles indicate the compounds that faulted during transformation [a, ice I→II; b, $\alpha\rightarrow\beta$ $Mg_2GeO_4$; c, calcite→aragonite; d, α-quartz→coesite; e, albite→jadeite+quartz; f, B1→B2 Rbl]. The dashed line is a postulated demarcation of fields of stable bulk transformation and unstable (transformational faulting) behavior. Mantle transformations of ferromagnesian composition, $(Mg_{0.89}Fe_{0.09})_2SiO_4$, are plotted as squares [1, $\alpha\rightarrow\beta$; 2, $\beta\rightarrow\gamma$; 3, $\alpha\rightarrow\gamma$; 4, $\alpha\rightarrow\gamma$ Fayalite; 5, γ→magnesiowustite+perovskite]. Calculation of $\Delta V/V_o$ and $\Delta T/T_m$ as described in the text.

tion (*75, 76*), provided that the higher melting temperature for silicate olivine and larger grain size for natural peridotites are taken into account (*82*). The uncertainty in this estimate of the kinetic limit for metastable olivine is about ±100°C. The narrow β-phase equilibrium field and the steep kinetic line indicate that the subducting lithosphere should largely bypass significant β-phase growth in the coldest part of thick subducting slabs (*83*).

Are there mantle phase transformations that have thermodynamic properties favorable for transformational faulting? The direct meta-stable olivine→spinel transformation for composition $(Mg_{0.89}Fe_{0.11})_2SiO_4$ has nearly the same latent heat and volumetric strain properties as the $Mg_2GeO_4$ olivine→spinel (α→γ) transformation, whereas the olivine→modified spinel (α→β) and modified spinel→spinel (β→γ) transformations have relatively low latent heats and smaller volume changes (Fig. 6). The reactions producing garnet and ilmenite from pyroxenes involve broad intermediate multiphase stability fields and have low Clapeyron slopes (*84*), both of which are stabilizing, as discussed above. The high-pressure reactions producing silicate perovskites from spinel, from (Mg,Fe)-$SiO_3$ ilmenite structure or from garnet (majorite) are all endothermic because of the unusually high entropy of the perovskite phase (*85*). All but the ilmenite→perovskite transformation involve multiple reactants or products, and are likely to be rate-limited by diffusive processes. For both reasons, reactions producing perovskites do not have properties favorable for transformational faulting. In summary, only the metastable olivine→spinel transformation has properties consistent with those of mineral systems that deform by transformational faulting in the laboratory (*86*). In support of this conclusion, Green and others (*87*) recently reported the formation of a transformational fault in a high-pressure experiment on silicate olivine. Compressional microinclusions of β-phase were produced during deformation, and an unidentified high-density fine-grained phase was localized in the fault zone. No mechanical data are available, and it is not known if unstable behavior occurred.

If conditions of extreme metastability occur in the olivine wedge (Fig. 8), are shear stresses high enough for faulting to occur? The prevailing view is that negative buoyancy forces due to higher slab density not only drive the descent of the cold lithosphere but also, in concert with viscous forces resisting plate penetration, create non-hydrostatic stresses that may cause deep earthquakes. Differential stresses due to resistive and buoyancy forces are generally estimated to be less than 0.3 GPa (*8, 15, 88, 89*).

Phase transitions with significant volume changes can have large effects on the state of stress near the transformation site. Woodward (*90*) showed by numerical modeling of an equilibrium distribution of olivine and spinel in subducting lithosphere that the transformation volume changes produce stresses in slab interiors that are much larger than those due to negative buoyancy of cold, dense slabs. Goto and co-workers (*91*) simulated the stress state in a subducting slab using the Sung and Burns (*32*) model of the olivine→spinel transition. They showed that the volume reduction to β-phase and spinel that occurs in the envelope of warmer subducting lithosphere around the cold unreacted olivine-rich core imposes layer-parallel compression on the wedge and deviatoric tension on the spinel-rich envelope (Fig. 8, inset) (*92*). Differential stresses in the wedge average about 1 GPa and increase as the wedge thins to a maximum of about 2 GPa. The most important uncertainties in their model are the thickness of the zone over which transformation takes place and the degree of viscous relaxation expected in the slab. The compressive state of stress in the wedge is in agreement with that inferred from the radiation patterns of deep earthquakes (*12, 40–42*). Transformation-induced stresses, unlike stresses associated with slab-negative buoyancy, do not require the slab to transmit forces over its length, which may be as much as 13 times its thickness.

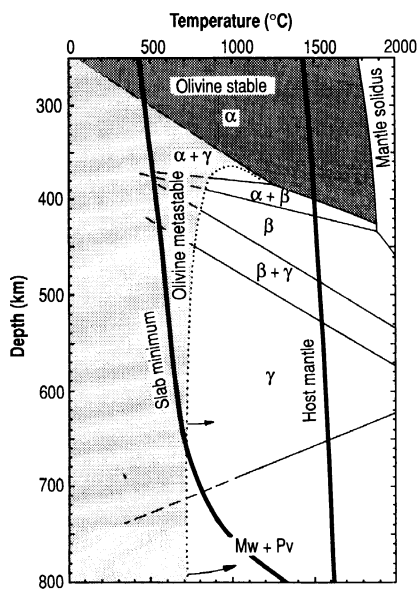


**Fig. 7.** Phase diagram and temperature distribution for the mantle, emphasizing the phase relations for the composition $(Mg_{0.89}\text{-}Fe_{0.11})_2SiO_4$. Equilibrium lines from (*3*) and the range of temperatures from the subduction thermal model of northeastern Japan by Helffrich *et al.* (*9*), augmented by data from Stein (*114*) for depths below 500 km. Also shown is the approximate kinetic line for 50% transformation to the stable assemblage (dotted) [after (*32*)]. Arrows indicate the expected direction of pressure effect on the kinetic line (*74*). The regions of olivine stability (dark stipple) and metastability (light stipple) are also shown. Increasing the slab thermal parameter, ϕ, shifts the slab-minimum temperature curve to the left, increasing the region of olivine metastability.

## Implications and Tests of the Unified Hypothesis

Are the estimated pressure-temperature-time paths in the metastable olivine wedge (Fig. 7) consistent with those expected in SZs that have deep earthquakes? Analytical models of the thermal evolution of the lithosphere show that isotherms are advected downdip in SZs approximately in proportion to the product of the age, $A$, of the lithosphere being subducted and the convergence rate normal to the SZ, $V_n$ (*34*). The distance that a particular isotherm is displaced down dip, $L$, is given by

$$L = kAV_n \tag{1}$$

where $k$ is a constant. Adiabatic heating is neglected. Down-dip lengths of SZ seismicity generally increase with the product $AV_n$. This is crudely consistent with maximum depths of earthquakes being controlled by a critical temperature (*34*). When the temperature of slab interiors rises above a critical value, slabs become too weak and stresses relax too fast to support earthquakes (*7–9, 27*). The SZs with the deepest seismicity are those subducting older (>80 Ma) and therefore thicker lithosphere at generally faster rates (>60 mm/a) (*35, 93*); these slabs are expected to remain cold to greater depth. In detail, however, the fit of $L$ versus $AV_n$ is not very satisfactory (*34*). Also, the peak in deep seismic activity near the bottom of the distribution is at odds with a simple thermal-diffusion weakening model. Furthermore, Brodholt and Stein (*94*) combined thermal models with strength predictions based on a laboratory-derived flow law for olivine and showed that the lithosphere should remain strong well below the maximum depths of most SZ earthquakes.

We have therefore used Eq. 1 in slightly different form to explore how variations in SZ thermal structure influence maximum earthquake depth instead of the length of the seismic zone. The vertical distance $Z$ that a particular isotherm is displaced is given by $Z = L\sin(\delta)$ where δ is the slab dip and from Eq 1,

$$Z = kA[V_n\sin(\delta)] = k\phi$$

where $V_n \sin(\delta)$ is approximately the vertical descent velocity. The thermal parameter $\phi = A[V_n \sin(\delta)]$ is a measure of how cold an SZ is at a given depth due to thermal inertia, neglecting adiabatic heating and latent heats of transformation.

The overall relation between $Z_{max}$ and $\phi$ (Fig. 9) is discontinuous and incompatible with simple weakening of the slab by thermal assimilation. Two distinct populations of subduction zones are evident. Those SZs that lack deep seismicity have consistently low values of $\phi$. For $\phi < 500$ km, $Z_{max}$ increases steeply with increasing $\phi$, but for $500 < \phi < 3000$, $Z_{max}$ is approximately constant at $250 \pm 50$ km, evidently independent of $\phi$ (*95*). The central Aleutian SZ has the highest $\phi$ in this group lacking deep earthquakes. What is the coldest temperature in the critical depth interval 350 to 400 km where the first series of phase changes are expected to occur in this SZ? Because the kinetic phase boundary and the isotherms in thermal models of SZs are nearly parallel, even small uncertainties in either produce large uncertainties in the predicted occurrence and maximum depth of the wedge (Fig. 8). Nonetheless, two recent numerical models predict that minimum temperatures in this slab at this depth may be ~650° to 750°C (*94, 96*). These conditions are at the onset of olivine metastability. The SZs with lower $\phi$ are warmer and therefore unlikely to develop significant olivine metastability and have transformational faulting-type earthquakes. Temperatures are probably high enough for transformations to $\beta$ and $\gamma$ phases to proceed at nearly equilibrium conditions in these SZs.

The SZs with $\phi > 3000$ km all have deep earthquakes. Why is this transition to this deep population so sharp? Over the range of $\phi = 3000$ to 4000, seismicity deepens from about 200 km in Sumatra to over 550 km near the Sunda Straight at 105°E and then deepens more gradually to over 650 km east of the Straight. A similar transition (not shown) occurs in the New Zealand–Kermadec–Tonga SZ between about 32° and 27°S, where earthquake depths increase from about 300 km to more than 600 km as $\phi$ increases from 4700 to 5600 km. We associate this pattern with the deepening of the metastable olivine-peridotite wedge that is controlled by the intersection of the kinetic line and the slab-minimum temperature (Fig. 7). The position of the slab-minimum temperature decreases as $\phi$ increases. Because of the steepness of the kinetic line, a small decrease in the slab-minimum temperature with increasing $\phi$ above about $\phi = 3000$ km results in a large increase in the depth of olivine-peridotite metastability.

The maximum depth of earthquakes of about 600 to 700 km for $\phi > 6000$ km does not change much over a wide range of values of $\phi$. One possible explanation is that the thermal parameter $\phi$ is inappropriate for lithosphere more than ~80 million years old. Seafloor of greater age does not subside significantly because of thermal contraction; lithosphere may have reached thermal equilibrium (*97, 98*). All of the subduction zones with $\phi > 6500$ have plate ages greater than 100 million years old, so plate temperatures may not be decreasing appreciably with increasing $\phi$ above 6500 km.

The steepness of the descent of seismic activity in the Indonesian and Tonga-Kermadec SZs with increasing $\phi$ and the abrupt change in slope at depths >600 km suggest that other factors contribute to the maximum in earthquake depths for these SZs. Some SZs show evidence of horizontal deflection when reaching depths of 550 to 680 km, on the basis of earthquake locations, focal mechanisms, or seismic velocity anomalies. These include some segments of Izu Bonin (*99, 100*), Kurile (*99*), and New Hebrides (*99*) SZs and the eastern Banda Sea segment of the Indonesian SZ (*101*). Occasionally deep earthquakes occur as much as 100 to 300 km outboard of the nearest Wadati-Benioff zone (*12, 102*). These events could represent lithosphere detached from the present-day SZ or their antecedents (*27, 103*). Detached or not, it is evident why earthquakes in some

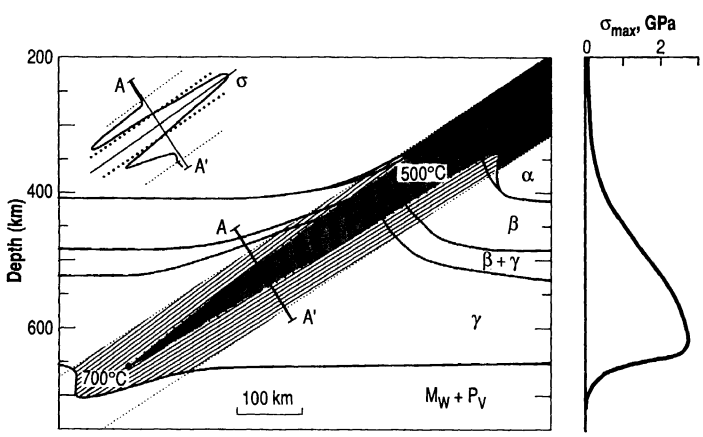


**Fig. 8.** (**Left**) Cross section showing the distribution of ferromagnesian silicate phases in subducting lithosphere based on the temperature distribution and phase relations summarized in Fig. 7. The maximum depths of the 500°, 600°, and 700°C isotherms are shown as filled circles. Also shown are the stability field of olivine (dark stipple), the equilibrium $\alpha \rightarrow \alpha + \gamma$ and the $\alpha \rightarrow \beta$ boundaries (dashed lines in the wedge), a wedge of metastable olivine peridotite (*32*) (light stipple), and regions of $\beta$– and $\gamma$-phase growth and stability in the slab (ruled). The thin $\alpha + \beta$ stability field is drawn as a single line. Depth extent of olivine metastability depends on the specific thermal structure, increasing as the plate thermal parameter $\phi$ decreases (Fig. 1). Inset: The wedge-parallel compressive stress in the metastable olivine wedge derives from the transformation strains in the envelope of lithosphere in which olivine has already transformed to spinel. (**Right**) Maximum differential stress parallel to plate and inside wedge. Both stress profiles summarized from (*91*).

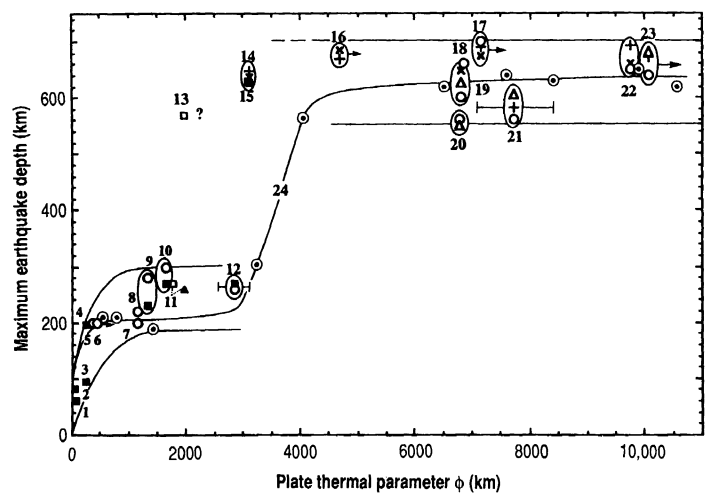


**Fig. 9.** Variation in maximum earthquake depth in individual SZ's with plate thermal parameter, $\phi$. Continuous line labeled "24" shows the variation of maximum earthquake depth along the Indonesian subduction zone from 97.9° to 126.3° E longitude showing that the transition occurs abruptly between $\phi = 3000$ and 5000 km. Arrows indicate SZ's with vigorous back-arc spreading, for which the plotted value of $\phi$ is an underestimate. See text and (*114*): 1, South Chile (50°S); 2, Cascadia (Pacific Northwest); 3, South Mexico; 4, South America (N. Ecuador and W. Colombia, 2° to 5°N); 5, Lesser Antilles, 6, Scotia (South Sandwich), 7, South America–Central Chile (30°S); 8, Indonesia-Sumatra; 9, Middle America; 10, Ryuku; 11, New Zealand; 12, Central Aleutians; 13, New Zealand "deeps" (39°S); 14, South America (Brazil, Peru); 15, S. America (North Argentina and South Bolivia); 16, New Hebrides; 17, Tonga; 18, N. Kermadec (23° to 27°S); 19, Kurile-Kamchatka; 20; Izu-Bonin; 21, Northwest Japan; 22, Indonesia (Banda Sea 120° to 126°E); 23, Marianas; 24, Indonesia (described above). Not shown are SZs for which plate age or convergence rates are highly uncertain or for which SZ geometry or history is complex. Earthquake data: + (*14*); x (*13*); ○ (*15*); △ (*99*); □, Adams and Ferry (*99*); ▲, various sources; ⊙, Yamaoka *et al.* (*114*); ■, Burbank and Frohlich (*114*).

SZs do not occur deeper than 600 to 700 km if lithosphere is deflected or has foundered at those depths.

In other SZs, like the western Brazil-Peru segment of the South America SZ (*95*), the Marianas SZ, the western Sunda segment of the Indonesia SZ, some segments of the Kurile SZ, and part of the Tonga SZ (*99*), the region of deep seismicity is steeply inclined and deflection near 650 km is not evident, even though descent rate is rapid and has been, in some cases, for tens of millions of years. The fate of the descending lithosphere in these SZs is controversial (*104–107*). If descent into the lower mantle does occur, this depth limit may indicate the maximum depth at which metastable olivine can transform to spinel in subducting slabs or, more likely, the beginning of formation of magnesiowüstite plus perovskite instead of spinel from metastable olivine (*108*). The equilibrium depth of the spinel→magnesiowüstite + perovskite transformation varies from ~650 to 710 km (Fig. 7), depending on the thermal structure. The rates of this reaction under deep slab conditions are unknown. However, velocity discontinuities have been identified at depths between 650 to 720 km for the Tonga slab; these observations suggest that this transformation occurs at close to equilibrium conditions in the Tonga SZ (*109*). If this interpretation is correct, then earthquakes abruptly terminate at about the same depth that mantle transformations have run to completion in the subducting slab, and the $\alpha \rightarrow \gamma$ transformational faulting mechanism cannot occur at greater depth, regardless of the stress state (*18, 19, 110*). Thus the cessation of seismic activity at about 690 km should not be used as an argument against plate penetration below that depth.

The idea that mantle phase changes in SZs play a dual role in generating nonhydrostatic stresses and, under metastable conditions, facilitate a deep shear instability can account for other characteristics of deep earthquakes: (i) "Rogue" deep earthquakes (*12*), located far from present-day SZs may be occurring in detached fragments of lithosphere from earlier regimes of subduction (*95*) that have not reached thermal and thermodynamic equilibrium. A local stress state connected with metastable transformations in such fragments is more plausible than one connected with buoyancy forces. (ii) The peaks in earthquake activity, sizes and total seismic energy release near the bottom of the distribution may be caused by the larger nonhydrostatic stresses at the tip of the metastable wedge (*91*) (Fig. 8). The pressure overstep for the $\alpha \rightarrow \gamma$ transformation also increases with depth. Olivine is therefore increasingly metastable. Alternatively, viscous creep resistance to plate penetration may increase markedly in the lower mantle. (iii) The small isotropic components of the radiation field compared to the shear component observed in SZs (*12, 44*) are also a characteristic of transformational faults. Transformational faults in the laboratory are thin compared to their lengths, and measured shear displacements along them are far greater than the calculated displacements resulting directly from the volume change. The basic potential energy source comes from the forces that create the nonhydrostatic stress state, not directly from the local release of free energy [compare with Liu (*30*)]. Stresses stored elastically in the metastable olivine wedge can originate from transformation in the spinel-rich envelope or from buoyancy forces, but the basic transformational-faulting energy source in the metastable olivine wedge is external to the fault. (iv) The occurrence of approximately volume-conserving non-double-couple source mechanisms may reflect multiple transformational faults of different azimuthal orientation (*38, 39*), as occasionally observed in experiments on ice. (v) The lack of specific seismic evidence for deep-plate bending deformation and the coherence of the down-dip compressive stress state inferred from the radiation patterns of deep earthquakes may be a consequence of the wedge structure (Fig. 8). Even though studies of many deep SZs suggest that many subducting plates are bent and sometimes contorted (*11, 91*), stress states inferred from inversions of seismic waveforms usually do not reflect comparable complexity. Compressional and extensional bending strains are highest near the top and bottom slab surfaces and lowest in the interior (*111*), near the olivine wedge. The slab is warmest near its top and bottom surfaces, and transformational faulting cannot occur there because olivine has already transformed to its denser polymorphs. Bending deformations are evidently accommodated aseismically. (vi) The absence of numerous deep aftershocks distributed on a main-shock fault plane is not surprising. Shallow aftershocks have been attributed to the presence and effects of water (*20*), factors that are not intrinsic to transformational faulting.

The presence of a deep, thin metastable olivine wedge would reduce negative buoyancy associated with the density contrast between the slab and the surrounding mantle. Such a reduction is partially offset by the elevation of the boundaries for $\beta$ and $\gamma$ phases in the warmer reacted envelope around the wedge. The wedge is also a thin, low-velocity channel and would be a guide for high-frequency seismic waves generated at deep earthquake sources. This structure might explain why strong defocusing effects expected from high-velocity slabs are generally not observed (*105*). Moreover, the difficulty in detecting positive velocity anomalies at depths below 300 to 400 km in SZs with deep seismicity might be in part attributed to the effects of the wedge structure.

Many aspects of the model bear closer scrutiny. Improved estimates of the kinetics of mantle phase transformations are needed as well as better thermal models in order to predict more reliably the distribution of transformations in SZs. More detailed seismic investigations of the velocity and phase distributions in deep SZs are also required. An exploratory experiment on silicate olivine that faulted (*87*) is partial confirmation of the hypothesis, but better controlled very high pressure deformation experiments are needed on olivine. The conditions that favor faulting instability in the laboratory may not necessarily apply to the earth. Only a full modeling study, as constrained by experiments, is capable of establishing the criteria for instability, where relevant boundary conditions of the subducting lithosphere, physical feedbacks involved in the stability (*86*), and relevant physical properties are all known. The lower half of the slab probably has more pyroxene and less olivine than the upper half (*112*), a mineralogic stratification that may tend to localize transformational faults in the upper part of the lithosphere. Finally, the geometry, thermal structure, phase distribution, and stress state implied by the model (Fig. 8) are obviously simplifications of the physical states of most deep subduction zones. The stress state in detail is a superposition of viscous forces, buoyancy forces, and thermodynamic forces that in any one subduction zone can result in quite complex stress states.

## Summary

In 1945, Bridgman (*24*) speculated on the possible roles of solid-solid phase changes in the occurrence of deep earthquakes and identified two important properties of solid-solid transformations relevant to deep earthquakes. Bridgman used the $H_2O$ ice phase transitions, such as the ice I→II transformation, as analogues for transformations in silicates. He pointed out that if a phase change is directly involved in the source mechanism of deep events, then it must run rapidly. This requires that the low-pressure phase be metastable (that is, the reaction must be overdriven in pressure) and that the reaction be exothermic to help promote runaway reaction rates. Bridgman also suggested that heterogeneous transformations involving large volume changes can produce nonhydrostatic stresses that could cause deep earthquakes. These are important elements of

the present hypothesis. It is indicative of Bridgman's foresight that more than 40 years later, deformation experiments on the metastable ice I→ice II transformation and other low-pressure transformation analogues have also revealed a new type of faulting instability that is also likely to be a key process in the deep earthquake environment.

REFERENCES AND NOTES


1. L.-g. Liu and W. Bassett, *Elements, Oxides and Silicates: High-Pressure Phases with Implications for the Earth's Interior* (Oxford Univ. Press, New York, 1986).
2. α olivine–β phase–γ spinel: T. Katsura and E. Ito, *J. Geophys. Res.* **94**, 15,663 (1989); γ spinel→Mw magnesiowüstite+Pv perovskite: E. Ito and E. Takahashi, *ibid.* **94**, 10,637 (1989); B. Wood, *ibid.* **95**, 12,681 (1990).
3. M. Akaogi, E. Ito, A. Navrotsky, *ibid.* **94**,15,671 (1989).
4. M. Niazi and D. L. Anderson, *ibid.* **70**, 4633 (1965); D. L. Anderson, *Science* **157**, 1165 (1967); L. Johnson, *J. Geophys. Res.* **72**, 6309 (1967); C. Archambeau, E. Flinn, D. Lambert, *ibid.* **74**, 5825 (1969); A. Dziewonski and D. L. Anderson, *Phys. Earth Planet. Inter.* **25**, 227 (1981).
5. P. Shearer, *Nature* **344**, 121 (1990); B. Wood and G. Helffrich, *ibid.*, p. 106; see recent reviews: C. Bina and B. Wood, *J. Geophys. Res.* **92**, 4753 (1987); C. Bina, *Rev. Geophys.*, in press.
6. The upper mantle is generally thought to be 50 to 80% olivine [see D. Weidner and E. Ito, in *High Pressure Research in Mineral Physics*, M. Manghnani and Y. Syono, Eds. (*Geophys. Monogr. 39*, American Geophysical Union, Washington, DC, 1987), p. 439; T. Irfune and A. E. Ringwood, *ibid.*, p. 231].
7. D. McKenzie, *Geophys. J. R. Astron. Soc.* **18**, 1 (1969); *Tectonophysics* **110**, 357 (1970); E. Oxburgh and D. Turcotte, *Geol. Soc. Am. Bull.* **81**, 1665 (1970); D. T. Griggs, in *The Nature of the Solid Earth*, E. Robertson, Ed. (McGraw-Hill, New York, 1972), pp. 361–384; N. Toksöz, J. Minear and B. Julian, *J. Geophys. Res.* **76**, 391 (1971); M. N. Toksöz, N. Sleep, A. Smith, *Geophys. J. R. Astron. Soc.* **35**, 285 (1973).
8. G. Schubert, D. Yuen, D. Turcotte, *Geophys. J. R. Astron. Soc.* **42**, 705 (1975).
9. J. Oliver and B. Isacks, *J. Geophys. Res.* **72**, 4259 (1967); D. Davies and D. McKenzie, *Geophys. J. R. Astron. Soc.* **18**, 51 (1969); E. Engdahl, N. Sleep, M. Lin, *Tectonophysics* **37**, 95 (1977); G. Bock, *Phys. Earth Planet. Inter.* **25**, 360 (1981); S. Roecker, *J. Geophys. Res.* **90**, 7771 (1985); T. Nieman, K. Fujita, W. Rodgers, Jr., *J. Phys. Earth* **34**, 43 (1986); E. Engdahl and D. Gubbins, *J. Geophys. Res.* **92**, 13,855 (1987); G. Helffrich, S. Stein, B. Wood, *ibid.* **94**, 753 (1989).
10. K. Wadati, *Geophys. Mag.* (*Tokyo*) **1**, 162 (1928); *ibid.* **8**, 305 (1935); L. Sykes, *J. Geophys. Res.* **71**, 2981 (1966).
11. D. Giardini and J. Woodhouse, *Nature* **307**, 505 (1984).
12. C. Frohlich, *Annu. Rev. Earth Planet. Sci.* **17**, 227 (1989).
13. P. Stark and C. Frohlich, *J. Geophys. Res.* **90**, 1859 (1985).
14. B. A. Rees and E. A. Okal, *Pageoph* **125**, 699 (1987).
15. M. Vassilou and B. Hager, *ibid.* **128**, 547 (1988); M. Vassilou, *Earth Planet. Sci. Lett.* **69**, 195 (1984).
16. This peak also is evident in the variations of energy release and cumulative earthquake moments [A. McGarr, *J. Geophys. Res.* **82**, 256 (1977); K. Abe and H. Kanamori, *ibid.* **84**, 3589 (1979); F. M. Richter, *ibid.*, p. 7683.
17. D. T. Griggs and J. Handin, in *Rock Deformation, Memoir 79*, D. T. Griggs and J. Handin, Eds. (Geological Society of America, New York, 1960), pp. 347–364; D. T. Griggs and D. Baker, in *Properties of Matter Under Unusual Conditions*, H. Mark and S. Fernback, Eds. (Wiley-Interscience, New York, 1969), pp. 23–42.
18. S. H. Kirby, *J. Geophys. Res.* **92**, 13,789 (1987).
19. H. Green and P. Burnley, *Nature* **338**, 753 (1989); P. Burnley, H. Green, D. Prior, *J. Geophys. Res.* **96**, 425 (1990).
20. C. Scholz, *The Mechanics of Earthquakes and Faulting* (Cambridge Univ. Press, Cambridge, 1990).
21. C. B. Raleigh and M. Paterson, *J. Geophys. Res.* **70**, 3965 (1965); C. B. Raleigh, *Geophys. J. R. Astron. Soc.* **14**, 113 (1967).
22. B. Hobbs and A. Ord, *J. Geophys. Res.* **93**, 10,521 (1988).
23. C. Meade and R. Jeanloz, *Eos* **70**, 1321 (1989); *Nature* **339**, 616 (1989); J. Lomnitz-Adler, *J. Phys. Earth* **38**, 83 (1990).
24. P. W. Bridgman, *Am. J. Sci.* **243A**, 90 (1945).
25. F. Evison, *Bull. Seismol. Soc. Am.* **53**, 873 (1963); M. Randall, *ibid.* **54**, 1291 (1964); J. Dennis and C. Walker, *Tectonophysics* **2**, 401 (1965); C. Walker and J. Dennis, *Nature* **209**, 182 (1966).
26. D. L. Anderson, *Science* **157**, 1165 (1967).
27. B. Isacks, J. Oliver, L. Sykes, *J. Geophys. Res.* **73**, 5875 (1968).
28. A. E. Ringwood, *Phys. Earth Planet. Inter.* **3**, 109 (1970); *Earth Planet. Sci. Lett.* **14**, 233 (1972).
29. N. Vlaar and M. Wortel, *Tectonophysics* **32**, 331 (1976).
30. L. Liu, *Phys. Earth Planet. Inter.* **32**, 226 (1983); see also McGarr (*16*)
31. L. Sykes, *J. Geophys. Res.* **73**, 1508 (1968).
32. C.-M. Sung and R. G. Burns, *Tectonophysics* **31**, 1 (1976).
33. J. Vaišnys and C. Pilbeam, *J. Geophys. Res.* **81**, 985 (1976).
34. P. Molnar, D. Freeman, J. Shih, *Geophys. J. R. Astron. Soc.* **56**, 41 (1979).
35. D. Rubie, *Nature* **308**, 505 (1984).
36. G. Helffrich and J. Brodholt, in preparation.
37. See discussions in (*12*); C. Frohlich, *J. Geophys. Res.* **92**, 13,777 (1987); *Sci. Am.* **260**, 48 (January 1989).
38. D. Giardini, *Geophys. J. R. Astron. Soc.* 77, 883 (1984).
39. Non–double-couple shallow and deep earthquake sources are not uncommon [D. Giardini, *Geophys. J. R. Astron. Soc.* 77, 883 (1984)]; some large deep events with non–double-couple radiation patterns have been interpreted and successfully modeled as nearly simultaneous multiple-faulting events: M. Randall and L. Knopoff, *J. Geophys. Res.* **75**, 4965 (1970); R. Strelitz, *Phys. Earth Planet. Inter.* **21**, 83 (1980); G. Choy and J. Boatwright, *Bull. Seismol. Soc. Am.* **71**, 691 (1981); K. Kuge and H. Kawakatsu, *Geophys. Res. Lett.* **17**, 227 (1990); (*12, 38*).
40. B. Isacks and P. Molnar, *Rev. Geophys.* **9**, 103 (1971) and references therein.
41. K. Apperson and C. Frohlich, *J. Geophys. Res.* **92**, 13,821 (1987).
42. S. Billington and B. Isacks, *Geophys. Res. Lett.* **2**, 63 (1975).
43. Y. Fukao, *Phys. Earth Planet. Inter.* **5**, 61 (1972); T. Sasatani, *J. Phys. Earth* **22**, 279 (1974).
44. E. Okal and R. Geller, *Phys. Earth Planet. Inter.* **18**, 176 (1979); M. Riedesel and T. Jordan, *Eos* **66**, 1080 (1985); D. Vasco and L. Johnson, *Geophys. J. R. Astron. Soc.* **97**, 1 (1989); H. Kawakatsu and K. Kuge, *Eos* **71**, 947 (1990).
45. H. Houston, *Seismol. Res. Lett.* **59**, 4 (1988); _____ and Q. Williams, *Eos* **71**, 1472 (1990).
46. R. Page, *J. Geophys. Res.* **73**, 3897 (1968); R. Willemann and C. Frohlich, *ibid.* **92**, 13,927 (1987).
47. Reconstructive phase transformations involve nucleation and growth of a new crystalline phase having no structural correspondence with the host phase.
48. P. W. Bridgman, *Proc. Am. Acad. Sci.* **47**, 441 (1912).
49. W. Durham, H. Heard, S. Kirby, *J. Geophys. Res.* **88**, B377 (1983); S. Kirby, W. Durham, M. Beeman, H. Heard, M. Daley, *J. Phys.* **48**, C1–227 (1987).
50. W. Durham, S. Kirby, H. Heard, L. Stern, *J. Phys.* **48**, C1–221 (1987); C. O. Boro, *J. Geophys. Res.* **93**, 10,191 (1988); S. Kirby, W. Durham, H. Heard, in *Ices in the Solar System*, J. Klinger *et al.*, Eds. (Reidel, Dordrecht, Holland, 1985), p. 711.
51. H. Heard, W. Durham, C. Boro, S. Kirby, in *The Brittle-Ductile Transition*, A. G. Duba, W. B. Durham, J. Handin, H. Wang, Eds. (*Geophys. Monogr. 56* American Geophysical Union, Washington, DC, 1990), p. 225.
52. Samples were cooled to below 130 K at pressure just after deformation, depressurized and then stored in liquid nitrogen. The presence of ice II was confirmed by cryogenic powder X-ray scans of sawcut and ground axial surfaces. The crystalline nature of the inclusions is also shown by the presence of grain-boundary grooves and grain faceting on the indium replicas. The absence of amorphous ice was not surprising because the pressures and normal stresses in our experiments were far lower than those required for its nucleation and stability [O. Mishima, L. Calvert, E. Whalley, *Nature* **310**, 393 (1984)]. We cannot exclude the possibility that amorphous ice formed in fault zones during faulting and then reverted to ice II during unloading, depressurization, and subsequent handling. The structure of ice II (rhombohedral space group $R\bar{3}$) has been determined by B. Kamb, W. C. Hamilton, S. J. LaPlaca, and A. Prakash [*J. Chem. Phys.* **55**, 1934 (1971)].
53. Green and Burnley (*19*) apply an "anticrack" model developed by R. Fletcher and D. Pollard [*Geology* **9**, 419 (1981)] to the displacement and stress fields around transformation inclusions. This model does not permit calculation of the variation of stresses and driving potential with position around the inclusion because stress singularities occur right where the interface moves fastest. The microinclusions of Green and Burnley, like those we see in ice, are curved at their tips rather than being sharp like cracks. As a technical term, "anticrack" also conveys an impression that these flaws have kinship with the physics of cracks and fracture, which they do not. We prefer to call them transformation flaws or compressional microinclusions.
54. S. Kirby, L. Stern, W. Durham, *Eos* **71**, 639 (1990); R. Fletcher and S. Kirby, *ibid.*, p. 639.
55. Neglecting pressure effects on entropy. $\Delta V$ is the volume change at pressure and stress.
56. Some of our earlier tests (*18, 49*) at >300 MPa and 77K showed faulting strength decreasing with increasing pressure. This may represent the onset of transformational faulting connected with transformation of ice I to high-density amorphous ice, as inferred from diamond-anvil experiments [R. Hemley *et al.*, *Nature* **338**, 638 (1989)].
57. C. Sammis and J. Dein, *J. Geophys. Res.* **79**, 2961 (1974).
58. D. Porter and K. Easterling, *Phase Transformations in Metals and Alloys* (Van Nostrand Reinhold, New York, 1981), p. 136; D. Rubie and A. B. Thompson in *Metamorphic Reactions: Kinetics, Texture and Deformation, Advances in Physical Geochemistry*, A. B. Thompson and D. Rubie, Eds. (Springer-Verlag, New York, 1985), vol. 4, p. 27. This possible latent heat effect is an additional destabilizing factor in the feedback between shear-strain localization and viscous heating discussed earlier as a possible deep earthquake source process [Griggs and Baker (*17*); M. Ogawa, *J. Geophys. Res.* **92**, 13,801 (1987)].
59. J.-P. Poirier, *Creep of Crystals* (Cambridge Univ. Press, Cambridge, 1985), pp. 213–228.
60. P. Burnley and S. Kirby, unpublished data.
61. M. Gilbert *et al.*, *Rev. Mineral.* **9B**, 229 (1982).
62. L. Dell'Angelo and S. Kirby, unpublished data.
63. C. Meade and R. Jeanloz, *Eos* **70**, 1321 (1989).
64. R. Geller, *Nature* **347**, 620 (1990).
65. D. Lockner, J. Byerlee, V. Kuksenko, A. Ponomarev, A. Sidorin, *ibid.* **350**, 39 (1991).
66. Z. Reches and D. Lockner, *Eos* **71**, 1586 (1990); Y. Du and A. Aydin, *Int. J. Numer. Anal. Methods Geomech.*, in press.
67. We estimated volume changes at $P$ and $T$ for a group of solid-solid transformations in minerals and ceramics from the molar volumes at standard conditions and their elastic and thermal-expansion properties. The latent heats were calculated as enthalpy changes at constant pressure from the Clapeyron equation, the slopes of the transition lines (*1*), the changes in molar volume and estimated temperatures

for potential faulting. Changes in these enthalpy values are conservative; latent heats in overdriven densification reactions are larger. We calculated the expected temperature increase $\Delta T$ by considering it as an adiabatic process and using the estimates of $\Delta H$ and the heat capacities of the product phases. We normalized the resulting $\Delta T$ by the ambient temperature of melting $T_m$ (*1*), in expectation that reaction rates and rates of plastic deformation, the processes likely to be influenced by latent heat, scaled with $T_m$ [H. J. Frost and M. F. Ashby, *Deformation Mechanism Maps* (Pergamon, Oxford, 1982), p. 133]. We also normalized the volume changes $\Delta V$ by the molar volume of the host phase $V_o$ at the equilibrium $P$ and $T$.

68. See data summary by J. Handin, in *Handbook of Physical Constants Memoir 79*, S. Clark, Jr., Ed. (Geological Society of America, New York, 1967), pp. 224–289; S. Kirby and J. McCormick, in *Handbook of Physical Properties of Rocks*, R. Carmichael, Ed. (CRC Press, Boca Raton, FL, 1984), vol. 3, pp. 139–280; H. Heard and C. B. Raleigh, *Geol. Soc. Am. Bull,* **83**, 935 (1972); B. Hacker and S. Kirby, *Eos* **71**, 1657 (1990).
69. J. A. Tullis, thesis, University of California, Los Angeles, CA (1971); (*62*).
70. B. Hacker and S. Kirby, *Eos* **71**, 639 (1990).
71. R. Wallat and J. Holder, *J. Phys. Chem. Sol.* **39**, 1147 (1978); W. Daniels and A. Skoultchi, *ibid.* **27**, 1247 (1966). Descriptions and illustrations of transformed specimens in these papers suggest that the *Fm3m*→*Pm3m* (B1→B2) transformation in Rbl is reconstructive in their experiments, not coherent.
72. B. Hacker and S. Kirby, unpublished data.
73. T. Ahrens and G. Schubert, *Rev. Geophys.* **13**, 383 (1975).
74. C.-M. Sung, *High-Pressure Science and Technology, vol. 2, Applications and Mechanical Properties*, K. Timmerhous and M. Barber, Eds. (Plenum, New York, 1979), p. 31.
75. R. Jeanloz, *J. Geophys. Res.* **92**, 10,352 (1987).
76. D. Rubie et al., *ibid.* **95**, 15,829 (1990); D. Rubie, S. Webb, A. Brearley, *Eos* **71**, 966 (1990).
77. D. Rubie, S. Webb, A. Brearley, *Eos* **71**, 966 (1990); *Nature* **348**, 628 (1990); A. Brearley, D. Rubie, E. Ito, *Phys. Chem. Minerals*, in press.
78. A. Remsberg, J. Boland, T. Gasparik, R. Liebermann, *Phys. Chem. Minerals* **15**, 498 (1988).
79. J.-P. Poirier [*High Pressure Research in Geophysics, Advances in Earth and Planetary Sciences* **12**, S. Akimoto and M. Manghnani, Eds. (Reidel, Dordrecht, 1982), p. 361] suggested that olivine transforms to spinel by a martensitic-like (coherent shear) mechanism, a mechanism that apparently occurs in the $Mg_2GeO_4$ $\alpha \rightarrow \gamma$ transformation at high shear stresses [P. Burnley and H. Green, *Nature* **338**, 753 (1989)]. This mechanism evidently does not occur in connection with transformation faulting in this same compound (*19*) nor in $Mg_2SiO_4$ at 900°C and above under nominally hydrostatic conditions (*76, 77*). Also there are no examples of martensitic transformations in metals or ceramics that are implicated in macroscopic shear instabilities and strain localization [compare with (*23*)].
80. A major part of this reduction in nucleation rates stems from the large strain-energy cost of nucleating new spinel when the host olivine has a large plastic yield strength, which increases steeply with decreasing temperature (*58, 74, 76, 77*).
81. T. Iidaka and D. Suetsugu, *Eos* **71**, 898 (1990); *ibid.*, p. 1574; in preparation.
82. The pressure effect is not included in the Sung and Burns (*32*) kinetic line and is likely to shift the reaction line to higher temperatures at the highest pressures (*58, 75*).
83. Transient metastable growth of spinel during pressurization at 900°C into the stability field of β-phase has also been observed in experiments on $Mg_2SiO_4$ (*77*).
84. M. Akaogi, A. Navrotsky, T. Yagi, S. Akimoto, in *High Pressure Research in Mineral Physics*, M. Manghnani and Y. Syono, Eds. *Geophys. Monogr. 39* (American Geophysical Union, Washington, DC, 1987), pp. 251–260.
85. A Navrotsky, *Geophys. Res. Lett.* **7**, 709 (1980); E. Ito and E. Takahashi, *J. Geophys. Res.* **94**, 10,637 (1989).
86. S. H. Kirby, *Eos* **70**,1316 (1989); *ibid.* **71**, 946 (1990).
87. H. W. Green II, T. E. Young, D. Walker, C. Scholz, *Nature* **348**, 720 (1990); _____, D. Prior, *Eos* **71**, 946 (1990).
88. G. Davies, *J. Geophys. Res.* **85**, 6304 (1980).
89. Some stress amplification is expected as the slab thins during heating, but the amount of amplification depends on the specific thermal model (*15*) and the rheology adopted [M. Wortel and N. J. Vlaar, *Pageoph* **128**, 625 (1988); Brodholt and Stein (*94*)].
90. D. Woodward, *Geophys. J. R. Astron. Soc.* **50**, 459 (1977).
91. K. Goto, H. Hamaguchi, Z. Suzuki, *Tectonophysics* **112**, 111 (1985); K. Goto, Z. Suzuki, H. Hamaguchi, *J. Geophys. Res.* **92**, 13,811 (1987).
92. Goto *et al.* (*91*) assume that the transformation strain is isotropic. If the bulk transformations are anisotropic under nonhydrostatic stress, as in the ice I→II transformation, then the stresses that accompany the transformation strain would be larger in the direction of the maximum compressive stress.
93. R. Jarrard, *Rev. Geophys.* **24**, 217 (1986).
94. J. Brodholt and S. Stein, *Geophys. Res. Lett.* **15**, 1081 (1988). A recent review of the rheology of olivine indicates that the parameter that describes the primary effect of pressure on olivine ductile strength, the activation volume $V^*$, is about 15 to 17 × $10^{-6}$ $m^3$ $mol^{-1}$ (C. Bai, S. Mackwell, D. Kohlstedt, *J. Geophys. Res.*, in press).
95. An exception to this pattern is the occurrence of a few New Zealand deep earthquakes even when $\phi < 2900$ km for the New Zealand SZ [R. Adams and B. Ferris, *N.Z. J. Geol. Geophys.* **19**, 269 (1976)]. These earthquakes are not understood in the context of the present hypothesis but could represent plate relicts from an earlier regime of subduction [M. Barazangi, B. Isacks, J. Oliver, J. Dubois, G. Pascal, *Nature* **242**, 89 (1973)]. Deep earthquakes in South America and in the New Hebrides SZs may also be detached from current subduction.
96. K. Creager and T. Boyd, *J. Geophys. Res.*, **96**, 2293 (1991) .
97. M. Renkin and J. Sclater, *ibid.* **93**, 2919 (1988).
98. See review by D. Hays, *ibid.*, p. 2937.
99. H.-w Zhou, *Phys. Earth Planet. Inter.* **61**, 199 (1990); *Geophys. J. Int.* **104**, 377 (1990).
100. M. Katsumata and L. Sykes, *J. Geophys. Res.* **74**, 5923 (1969).
101. R. Cardwell and B. Isacks, *ibid.* **83**, 2825 (1978); K. Newcomb and W. McCann, *ibid.* **92**, 421 (1987); R. Ghose and K. Oike, *Bull Disas. Prev. Res. Inst., Kyoto Univ.* **38**, 223 (1988).
102. G. Ekström, A. Dziewonski, J. Ibanez, *Eos* **71**, 1462 (1990).
103. M. Barazangi, B. Isacks, J. Oliver, J. Dubois, G. Pascal, *Nature* **242**, 98 (1973).
104. T. Jordan, *J. Geophys. Res.* **43**, 473 (1977); K. Creager and T. Jordan, *ibid.* **89**, 3031 (1984); *ibid.* **91**, 3573 (1986); P. Silver and W. Chan, *ibid.*, p. 13, 787; S. Kamiya and T. Miyatake, *Geophys. Res. Lett.* **15**, 828 (1988);_____, K. Hirahara, *Bull. Earthq. Res. Inst., U. Tokyo* **64**, 457 (1989); D. Suetsugu, *J. Phys. Earth* **37**, 265 (1989).
105. D. L. Anderson, *J. Geophys. Res.* **92**, 13,968 (1987); H.-W. Zhou and R. Clayton, *ibid.* **95**, 6829 (1990); H.-W. Zhou, D. L. Anderson, R. Clayton, *ibid.*, p. 6799; H. W. Zhou and D. L. Anderson, *Proc. Natl. Acad. Sci. U.S.A.* **86**, 8602 (1989).
106. J. Vidale, *Geophys. Res. Lett.* **14**, 542 (1987).
107. W. Spakman, S. Stein, R. van der Hilst, R. Wortel, *ibid.* **16**, 1097 (1989).
108. Such a transformation would not favor transformational faulting because the latent heat would be small, and because it is a phase-separation reaction (see text).
109. G. Bock and J. Ha, *Geophys. J. R. Astron. Soc.* **77**, 593, 1984; M. Richards and C. Wicks, *Geophys. J. Int.* **101**, 1 (1990) and references therein; C. Wicks and M. Richards, *Eos* **71**, 904 (1990).
110. D. Giardini and J. Woodhouse, *Nature* **319**, 551 (1986).
111. See, for example, D. Turcotte and G. Schubert, *Geodynamics: Applications of Continuum Mechanics to Geological Problems* (Wiley, New York, 1984), chaps. 3 and 7.
112. A. E. Ringwood, *Tectonophysics* **112**, 17 (1985).
113. S. Stein, personal communication.
114. Plate parameters used in calculating $\phi$ from various sources. Seismic data: sources indicated in caption and K. Yamaoka, Y. Fukao and M. Kumazawa, *Rev. Geophys.* **24**, 27 (1986); G. Burbach and C. Frohlich, *ibid.* **24**, 833 (1986). Plate age: G. Moore *et al.*, Circum-Pacific Map Project, Plate Tectonic Map of the Circum-Pacific Region (American Association of Petroleum Geologists, Tulsa, 1981), five sheets; see (*93, 97*), Convergence rates: RM2 model by B. Minster and T. Jordan [*J. Geophys. Res.* **83**, 5331 (1978)] compiled in Moore *et al.* and (*93*), corrected where required by the NUVEL-1 model of C. Demets, R. Gordon, D. Argus, S. Stein [*Geophys. J. Int.* **101**, 425 (1990)]. Plate dip below 150 km depth from the seismic sources indicated in caption and from (*93*). For SZs with deepest earthquakes at 200 km and shallower, dip angle was the average dip from the trench to the deepest earthquakes. Error bars vary with individual SZs, but the standard errors in $\phi$ generally vary as indicated for the Central-Aleutian and NE-Japanese SZs; standard errors for the deepest earthquake depth determinations also vary but generally depths are uncertain to 10 to 30 km.
115. We thank the following reviewers for their help improving this manuscript: A. McGarr, T. Hanks, B. Hacker, D. L. Anderson, J. Dieterich, C. Frohlich, S. Stein, and R. Geller. We also thank T. Iidaka, D. Suetsugu, A. Brearley, D. Rubie, and H. Kawakatsu for permission to quote their work in advance of publication.